Published in IET Radar, Sonar and Navigation
Received on 23rd January 2012
Revised on 17th April 2012
doi: 10.1049/iet-rsn.2011.0401

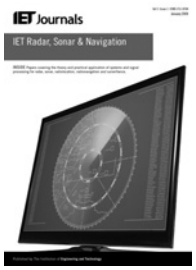

ISSN 1751-8784

Antenna array characterisation and signal processing for an FM radio-based passive coherent location radar system

F. Belfiori[1] *S. Monni*[2] *W. van Rossum*[2] *P. Hoogeboom*[1,2]

[1]*Geoscience and Remote Sensing, Delft University of Technology, Stevinweg 1, 2629CN Delft, The Netherlands*
[2]*TNO, Oude Waalsdorperweg 63, 2597AK The Hague, The Netherlands*
E-mail: f.belfiori@tudelft.nt

Abstract: The design of passive coherent location radar, which exploits broadcasting transmitters of opportunity in the very high frequency (VHF) radio bandwidth, is presented. Here, the authors primarily focus on the system set-up and on the digital pre-processing steps. Emphasis is given to the antenna section analysis. The eight-element circular array, which is used for the signal acquisition, is analysed by means of simulations and measurements. Compensation for the mutual coupling effect between the different channels is achieved by applying a technique in the digital domain. An innovative digital beamforming algorithm is introduced to reduce the sidelobe level of the circular array pattern. Direct path interference suppression, range/Doppler data processing, greatest-of constant false alarm rate algorithm and range/Doppler-time plots extraction provide the final output of the processing chain. Experimental validation of the processing architecture is presented and the final detection results are compared with an automatic dependent surveillance broadcast data set.

1 Introduction

The last decade has seen an increase in the interest for passive RF radar-based surveillance systems, conventionally referred to passive coherent location (PCL) systems, passive bistatic radar (PBR) and passive covert radar (PCR). In the following we will use the acronym PCL. The main idea behind these systems is to exploit non-cooperative transmitters and *ad hoc* deployed receivers to perform target localisation and tracking. Suitable illuminators of opportunity should be available at any time and operate in the same frequency region as the radar receiver. FM radio, analogue television and digital radio and television broadcasts are the most frequently used signals for this purpose [1–4]. The main advantages of PCL systems are similar to the ones of conventional bistatic radars [5, 6], but they present specific challenges that must be considered. First of all, the transmitter location and the waveform design cannot be controlled, leading to a certain degree of variability in the system performance. Furthermore, the acquisition of a clean reference signal and the rejection of the direct path interference (DPI) in the surveillance channel must be achieved [7, 8], otherwise it turns out to be an additive clutter signal capable to mask the presence of real targets.

Several research studies have been published on different topologies of PCL systems employing either a single receiver antenna [9] or receiver antenna arrays in linear [10] and circular [11] configurations. The benefit of antenna arrays resides on the possibility of applying digital beam forming (DBF) algorithms in order to steer and to shape the array radiation pattern. The use of a circularly shaped receiving array also provides no degradation of the pattern characteristics in relation with the steering angle, making this configuration more suitable for surveillance and tracking operations. On the other hand, because the same array is used to acquire both the direct signal coming from the broadcaster and the signal that is reflected by the target, a higher DPI suppression and a more careful analysis of the receiver's dynamic range (DR) is required with respect to the systems that use separate receiving channels. Furthermore, the application of DBF algorithms demands for an accurate calibration of the system; a compensation for the mutual coupling (MC) effects between the antenna elements is needed in order to optimise the beam shaping procedure.

An agile passive radar system has been developed with 360° surveillance capability on the azimuth plane, large detection ranges, with respect to expected passive system performance [7], and FM station independent. The system agility resides in the designed analogue receiver, which is capable of exploiting the full FM radio bandwidth. The selection of a specific channel, by means of the digital down conversion (DDC), can in principle be parallelised in order to acquire the information from different transmitters of opportunity. However, in the presented work the discussed calibration procedure has been developed and tested only for a single frequency channel. To further clarify our contributions to the PCL radar design and realisation, in this paper we: (i) describe the design for an

eight-element circular array and the calibration procedure that has been applied to it in the digital domain, (ii) introduce a novel DBF algorithm for the sidelobe reduction (SLR) which is independent of the geometric configuration of the array, (iii) show the implemented digital processing scheme for the realised FM PCL system and the achieved results. The paper is organised as follows. In Section 2 an overall description of the PCL system is provided, with specific attention to the characterisation of the radar analogue receiver. The antenna array is illustrated in Section 3, where the technique for the MC compensation is also described. Sections 4 and 5 present the DBF algorithm for the sidelobe suppression and the digital signal processing chain, respectively. Section 5 also shows results on detected aircrafts that are compared with automatic dependent surveillance-broadcast (ADS-B) data. Conclusions are drawn in Section 6.

2 PCL system overview

The receiver antenna consists of an eight-element circular array which is shown in Fig. 1. The signals received by the antennas are independently amplified and filtered by an eight-channel analogue receiver. The receiver presents frequency agility in the FM radio band. The system does not perform analogue down conversion to a lower frequency and the whole FM radio band is digitally converted. The analogue receiver was designed such to be flexible and reliable in different working environments, also in the presence of relatively strong unwanted signals. For this reason it has been equipped with several switchable attenuators. A simplified sketch of the receiver configuration is presented in Fig. 2.

Each receiving channel, as highlighted in Fig. 3, is composed by the following stages: (1) a 10 dB tuneable attenuator, which can be introduced if very strong signals are expected at the input of each channel, (2) a 20 MHz bandpass filter centred around 98 MHz that prevents intermodulation of strong incoming out-of-band signals with signals inside the FM-band; (3) a 10 dB pre-attenuator that can be used to reduce the total gain of the receiver if the input signals are so strong to cause saturation of the analogue to digital converter (ADC; this pre-attenuator is

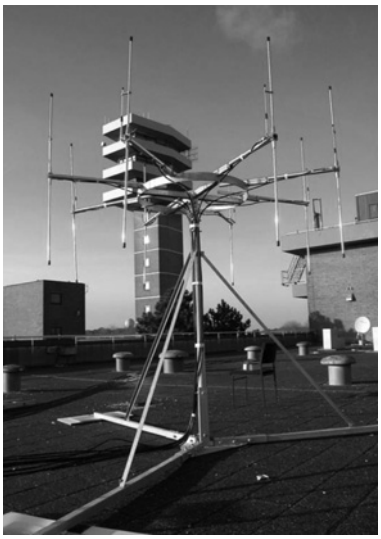

Fig. 1 *PCL array and, on the background, the TNO tower on top of which it is currently located*

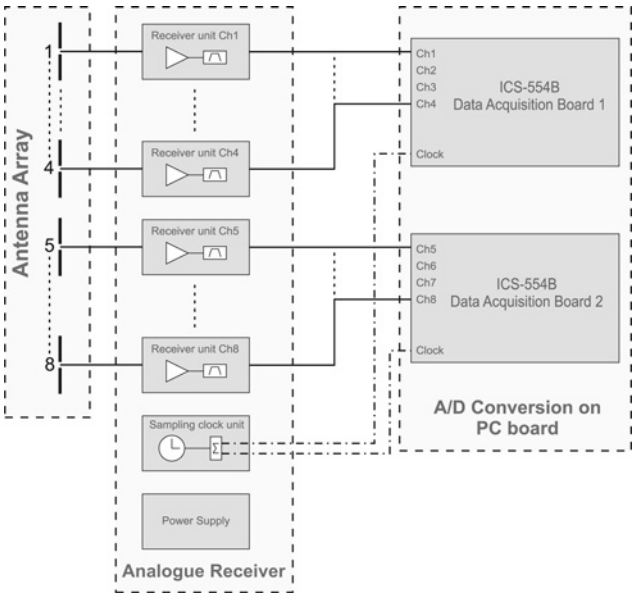

Fig. 2 *Simplified schematic of the passive radar receiver*

normally switched off); (4) a low-noise amplifier, which provides to the signal a 22 dB gain; (5) a high-pass filter with a cut-off frequency of 88 MHz, which suppresses the signals on the low side of the FM-band; (6) a fixed 6 dB attenuator that isolates the high- and low-pass filter; (7) a low-pass filter with a cut-off frequency of 108 MHz, which suppresses the signals on the high side of the FM-band; (8) a 10 dB post-attenuator whose purpose is to control the gain of the receiver and it does not influence the noise figure of the system; (9) a 22 dB gain amplifier; and (10) a fixed 6 dB attenuator that has three purposes: preventing the digitiser from being damaged by too strong signals from the amplifier; improving the S11 at the output of the receiver and providing a short-circuit protection to the receiver output. The analogue signals are then converted using 2 four-channel ICS-554B digitiser PC boards [12]. The nominal number of bits is 14 and the used sampling frequency is equal to 80 MHz.

2.1 Bandwidth and DR considerations

Owing to physical limitations in data handling and storage capacity of the digital section of the current system, the digitiser boards work in DDC mode. The DDC selects a specific channel (96.8 MHz carrier of FM3 radio from Lopik) which has a bandwidth of 250 kHz, therefore the filtering yields a decimation (reduction in signal bandwidth) of a factor 320 or 25 dB. A noise power reduction of 25 dB approximately corresponds to a gain in DR of 25 dB or 4 bits. Therefore the theoretically achievable DR after the DDC is 109 dB (18 bits).

A setback is that the suppression level of the out-of-band signals, F_{DDC} although large is still finite. The out-of-band signals are suppressed at the DDC output by about 70 dB (measured signal level relative to an injected out-of-band signal). By assuming a completely and uniformly filled FM band, the maximum power reduction factor F_{pow} is given by

$$F_{\mathrm{pow}} = \frac{F_{\mathrm{DDC}}(B_{\mathrm{FM}} - B_{\mathrm{channel}}) + B_{\mathrm{channel}}}{B_{\mathrm{FM}}} \simeq \frac{B_{\mathrm{channel}}}{B_{\mathrm{FM}}} \quad (1)$$

where B_{channel} is the bandwidth occupied by a single channel,

doi: 10.1049/iet-rsn.2011.0401

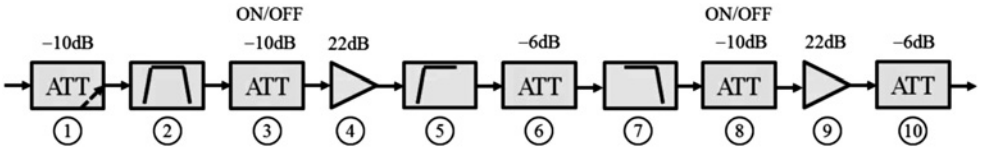

Fig. 3 *Block diagram of a receiving channel*

selected by the DDC, and B_{FM} is the whole FM bandwidth. However, the power distribution within the band of interest is not uniform and N_{ch} separate equal-power channels can be distinguished. According to that, (1) becomes

$$F_{pow} = \frac{F_{DDC}(N_{ch} - 1) + 1}{N_{ch}} \simeq \frac{1}{N_{ch}} \tag{2}$$

The N_{ch} value was estimated by considering all the stations for which the received power, measured at the input of the analogue receiver, was greater or equal to the Lopik value minus 3 dB. In our case this yields $N_{ch} = 20$ and a reduction factor of about 13 dB. Thus, after the DDC the thermal noise is reduced by a factor of 320 although the maximum expected power is reduced by a factor 20. This corresponds to an increase in DR of a factor 16 (12 dB) or 2 bits and not the expected increase of 4 bits from noise consideration alone. As a consequence, the actually available DR after the DDC is 96 dB (16 bits).

2.2 Power consideration about the broadcasting stations in the FM bandwidth

The maximum signal level at the ADC input corresponds to the total power received in the FM band at the passive radar location, a 40 m high tower at TNO premises in The Hague. Multiple transmitters and multiple stations operate in the FM band. In order to evaluate the impact of all these transmitters on the signal levels, an oscilloscope was used to estimate the amplitude of the signals received from each dipole. The time average power levels are depicted in Table 1.

With reference to the analysis illustrated in the previous section, the minimum gain provided by the receiving channel depicted in Fig. 3 is $G_{min} \simeq 6.5$ dB. According to the values in Table 1 and by considering that the maximum input power to the ADC, in order to avoid clipping effects, is 8 dBm (by experimental estimation) we concluded that at the current array location the tuneable attenuator could be set to 0 dB whereas both the pre-attenuator and the post-attenuator had to be switched on during the data acquisition.

From the radar point of view, this constraint has a high impact on the system performances as the noise figure of the whole system is degradated to the value, directly measured, of 17 dB. As a consequence, the detection sensitivity is also decreased because of the additional noise that is introduced.

3 Antenna array analysis

An extensive analysis of the antenna characteristics, for both the single radiating element and the overall array, has been conducted. The antenna is a circular array consisting of eight half-wavelength dipoles produced by Aldena (type AST.01.02.235). The dipole bandwidth defined with respect to a return loss of 10 dB is about 19% centred at the operating frequency within the FM band (88–108 MHz). Each dipole is equipped with a Gamma match which allows fine tuning the input impedance to optimise the matching at the operating frequency. This feature is useful when the antenna is inserted in an array environment because the MC affects the antenna input impedance. The dipoles have been tuned to operate at 96.8 MHz, the broadcast frequency of Radio 3 in the Netherlands, which has been selected as emitter of opportunity because of its high transmitted power (100 kW).

The measurements of the scattering parameters of the array have shown an overall behaviour which is below −10 dB in the bandwidth 88–102 MHz and below −8 dB in the bandwidth 102–108 MHz. A frequency agility of the array elements could also be appreciated. However, the calibration procedure that is described in this section is frequency dependent and the results are only valid at the reference frequency of 96.8 MHz.

3.1 Antenna element characterisation

Simulations of the antenna were carried out using an FDTD-based commercial software package: CST Microwave Studio [13]. Since the exact characteristics of the selected antenna were not disclosed by the manufacturer, a dipole of radius $r = 0.003\lambda$ and length $l = 0.45\lambda$, where $\lambda = 309.93$ cm at the frequency of 96.8 MHz, was considered for the simulations. The stand-alone behaviour changes when the radiating element is part of an array: the shorter the array radius with respect to the wavelength the further in frequency is the onset of grating lobes, but the higher is the MC. Moreover, the closer are the elements, the more directive the pattern becomes.

Different array configurations have been investigated by taking into account both the EM behaviour of the structure and the following signal processing steps. The multiple aspects have been analysed and as a result of this trade-off a radius $a = 0.48\lambda$ was chosen. The measurements aimed at evaluating the element pattern behaviour of the real system have shown a good matching with the simulations. Fig. 4 presents the results of the measurements on three different array elements in comparison with the element pattern obtained with the CST simulation. Element patterns have been evaluated in the array configuration and at the reference frequency of 96.8 MHz. The element pattern of the array elements has been characterised in an open air far-field measurement setup, by placing the array on a rotating

Table 1 Average power levels at the input of the analogue receiver

	Ch. 1	Ch. 2	Ch. 3	Ch. 4	Ch. 5	Ch. 6	Ch. 7	Ch. 8
power, dBm	2.54	1.34	2.46	2.73	2.78	−2.82	−6.49	0.38

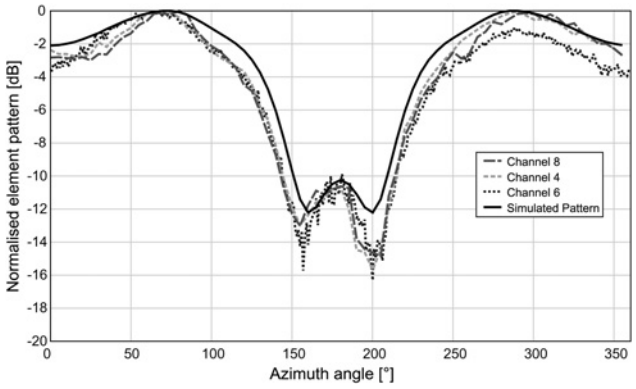

Fig. 4 *Comparison between the measured element patterns for three different array channels and the CST simulated data*

platform and using a biconical dipole antenna as reference transmitter.

In small arrays the element pattern is not the same for all elements. Each element pattern is affected by the presence of the other elements, therefore it depends on the position in the array. It has been shown in [14] that, for frequencies and angles for which single-mode operation is guaranteed, it is possible to compensate for the error because of the MC by multiplying the received signals by the inverse of the MC matrix. The related theory is briefly summarised in the following paragraph where the compensation technique, which has been used, is also highlighted.

3.2 MC effect and compensation technique

The array pattern of a conventional array can be expressed as a product of the element pattern and the array factor [15]. In real arrays, the element pattern is affected by the neighbouring elements and, if we refer to a uniform circular array (UCA), it is an angular function of the element position. The far-field array pattern for N-elements circular array can be written as

$$P(\phi) = \sum_{n=1}^{N} a_n f_n(\phi - \phi_n) \mathrm{e}^{\mathrm{j}kr\cos(\phi-\phi_n)} \tag{3}$$

where f_n is the element pattern affected by MC, a_n is the complex weight applied to the array element, $k = 2\pi/\lambda$ being λ the wavelength, r is the array radius, ϕ is the direction of an impinging monochromatic field with respect to the phase centre of the array and ϕ_n is the angular position of the nth element along the circumference. Similarly to [14], the total received voltage at the mth element can be written as a weighted sum of the contributions of the all array elements

$$\begin{aligned} v_m(\phi) &= c_{mm}E_m f_i(\phi - \phi_m) + \sum_{n,n\neq m}^{N} c_{mn}E_n f_i(\phi - \phi_n) \\ &= \sum_{n=1}^{N} c_{mn}E_n f_i(\phi - \phi_n) \end{aligned} \tag{4}$$

being E_m the electric field which excites the mth element port and f_i the ideal element pattern. The MC coefficient c_{mn} therefore represents the proportionality term which relates the induced voltage on channel m to the total voltage on channel n. The desired voltage on channel m is then given by

$$v_m^{\mathrm{d}}(\phi) = E_m f_i(\phi - \phi_m) \tag{5}$$

If we compare (4) and (5) and taking into account that $E_m = E_m \mathrm{e}^{\mathrm{j}kr\cos(\phi-\phi_m)}$ we obtain the same expression as [14] for the linear case which relates the desired voltage signal and the real (affected by MC) one. By means of a matrix notation

$$\boldsymbol{v}^{\boldsymbol{d}} = \boldsymbol{C}^{-1}\boldsymbol{v} \tag{6}$$

where the MC matrix $\boldsymbol{C}$ can also be written as a function of the antenna scattering parameters

$$\boldsymbol{C} = \boldsymbol{S} + \boldsymbol{I} \tag{7}$$

with $\boldsymbol{I}$ and $\boldsymbol{S}$ being the identity and the scattering matrix parameters, respectively.

The MC matrix can be calculated analytically or numerically, depending on the antenna type [15]. However, in real systems the cables and the analogue and digital front-end introduce discrepancies with respect to theoretical results. In the simplified hypothesis that the cable is a reciprocal structure, its effect on the expression of the coupling matrix can be written in terms of the diagonal matrix of the transmission coefficients of the cables $\boldsymbol{T}$ [14]

$$\boldsymbol{C} = \boldsymbol{T}(\boldsymbol{S} + \boldsymbol{I}) \tag{8}$$

Equation (8) fully describes the matrix term which must be applied in order to compensate for the non-ideal behaviour of the analogue section of the system. Since the presented correction is applied in the digital domain, for example after digital conversion of the received signals, the effect of the phase and amplitude errors introduced by the digital receiver should also be taken into account. The final correction matrix can then be expressed as the following product

$$\boldsymbol{C}_{\mathrm{f}} = \boldsymbol{P}[\boldsymbol{T}(\boldsymbol{S} + \boldsymbol{I})] \tag{9}$$

where $\boldsymbol{P}$ is the digital section compensation matrix. The $\boldsymbol{S}$ matrix was measured by means of a network analyser whereas the $\boldsymbol{P}$ matrix was estimated by connecting a stable transmitter to an eight-channel splitter which directly fed the digital receiver.

The expression retrieved in (9) is valid when no other signal sources, which can generate local interferences to the radiation pattern, are present in the array location. However, the environment in which the TNO passive radar is located, the top of the tower at The Hague laboratory, is heavily affected by multi-path because of the presence of several large metallic structures. Moreover, the signal received from local radio stations is relatively strong with respect to the signal chosen as reference, causing interference. For this reason, the $\boldsymbol{C}_{\mathrm{f}}$ matrix coefficients have been refined by means of an optimisation approach which is hereby described.

The $\boldsymbol{C}_{\mathrm{f}}$ matrix has been derived by measuring the signal received by the array elements although a transmitter is positioned around the array in known positions, as proposed in [11]. For a far-field monochromatic source, a generic received data vector can be written as

$$\boldsymbol{x} = \boldsymbol{C}_{\mathrm{f}}[\boldsymbol{s}\boldsymbol{a} + \boldsymbol{n}] \tag{10}$$

doi: 10.1049/iet-rsn.2011.0401

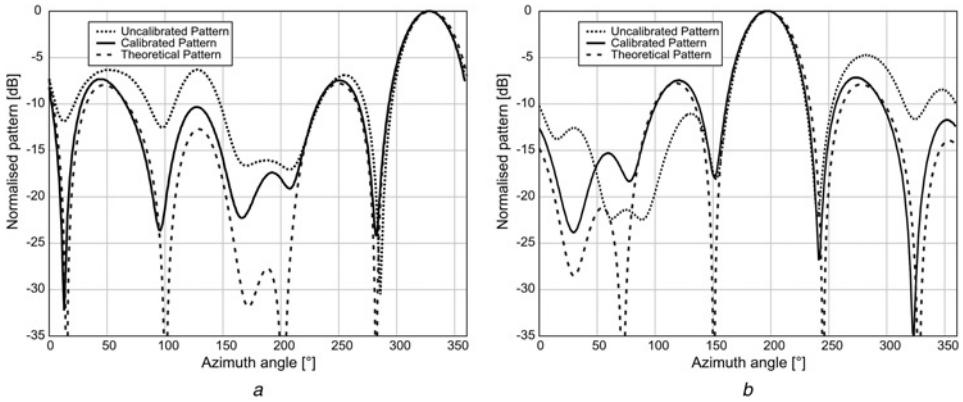

Fig. 5 *Cartesian reference system comparison between the un-/calibrated and the theoretical patterns in dB scale*

a Transmission point 1
b Transmission point 2

where a is the amplitude of the transmitted signal and $\boldsymbol{n}$ a noise realisation vector. The vector $\boldsymbol{s}$ is the steering vector of the array that, on the azimuthal plane for an angle of arrival ϕ_0, takes the form

$$\boldsymbol{s} = [e^{jkr\cos(\phi_0)}, e^{jkr\cos(\phi_0-\phi_1)}, \ldots, e^{jkr\cos(\phi_0-\phi_{N-1})}]^{\mathrm{T}} \quad (11)$$

where $(\cdot)^{\mathrm{T}}$ is the transposed operator. It must be noticed that the value ϕ_0 is known.

The data acquisitions have been performed at M transmission points, each of them theoretically characterised by the same coupling matrix. Thus, it is possible to write the following objective function

$$O(\boldsymbol{C}_f, a_1, a_2, \ldots, a_M) = \sum_{m=1}^{M} \|\boldsymbol{x}_m - \boldsymbol{C}_{\mathrm{f}}\boldsymbol{s}_{\mathrm{m}}a_{\mathrm{m}}\|^2 \quad (12)$$

which represents a non-linear system of equations whose unknowns are the signal amplitudes $[a_1, a_2, \ldots, a_M]$ and the coupling matrix elements in $\boldsymbol{C}_{\mathrm{f}}$. The $\boldsymbol{x}_{\mathrm{m}}$ vector is the collected data vector having the transmitter at the mth location around the array. A Broyden–Fletcher–Goldfarb–Shanno (BFGS) quasi-Newton method [16, 17] has been implemented to minimise the objective function in (12) and to retrieve $\boldsymbol{C}_{\mathrm{f}}$. Results of the compensation for two of the selected transmission points are depicted in Fig. 5. The array patterns have been measured by electronically steering the array.

Effects of the calibration include the removal of the pattern asymmetries and the reduction of the side lobe level to the expected theoretical value of -8 dB. If we compare the obtained figures, differences between the compensated diagrams mostly affect the region far from the main beam pointing. Such discrepancies depend on both the variability of the multi-path interferences with respect to the angular position of the transmitter, and the convergence of the optimisation algorithm which is mostly influenced by the main beam region, where the signal amplitudes are stronger.

4 DBF algorithm for the SLR

In passive radar applications the requirement on the SLL can be a very stringent constraint, as the power ratio between the reference signal and a target echo can be in the order of 100 dB. Thus the patterns obtained in the previous section are not able to satisfy it. A further reduction can be achieved by means of a non-uniform tapering on the array channels. In this section we firstly present a novel algorithm for the synthesis of low SLL circular array patterns and then we compare its performance with the one based on phase modes [18–20], which is specifically tailored for circular arrays.

4.1 Proposed DBF algorithm

The pattern of an UCA antenna can be written in a matrix notation from (3)

$$P(\phi) = \boldsymbol{s}^{\mathbf{H}}\boldsymbol{a}(\phi) \quad (13)$$

where the superscript $(\cdot)^{\mathbf{H}}$ represents the Hermitian operator, $\boldsymbol{a}(\phi)$ is the circular array manifold and the element pattern contribution has been removed for simplicity. The objective of a beamforming procedure is to identify the steering vector which minimises the contribution from the side lobes and focuses the energy in the main beam region. A considerable degradation of the angular resolution should also be avoided. These conditions can be translated, using (13), into the following optimisation problem

$$O(\boldsymbol{s}) = \min_{\mathbf{s}}\{\|\boldsymbol{s}^{\mathrm{H}}\boldsymbol{a}(\phi) - f_d(\phi)\|^2\} \quad (14)$$

where $f_d(\phi)$ is a mask function that describes a desired array pattern behaviour. Equation (14) can be rewritten as

$$O(\boldsymbol{s}) = \min_{\mathbf{s}}\{[\boldsymbol{s}^{\mathrm{H}}\boldsymbol{a}(\phi) - f_d(\phi)]\boldsymbol{\Lambda}[\boldsymbol{s}^{\mathrm{H}}\boldsymbol{a}(\phi) - f_d(\phi)]^{\mathrm{H}}\} \quad (15)$$

where $\boldsymbol{\Lambda}$ is a diagonal matrix of weights that are defined in order to emphasise the attenuation in the side lobe region. As a function of the steering vector $\boldsymbol{s}$, which is the only unknown in the second term of (15), the desired minimisation argument is obtained by imposing the equality to zero of the first-order derivative

$$\boldsymbol{a}(\phi)\boldsymbol{\Lambda}[\boldsymbol{s}^{\mathrm{H}}\boldsymbol{a}(\phi) - f_d(\phi)]^{\mathrm{H}} + [\boldsymbol{s}^{\mathrm{H}}\boldsymbol{a}(\phi) - f_d(\phi)]\boldsymbol{\Lambda}\boldsymbol{a}^{\mathrm{H}}(\phi) = 0 \quad (16)$$

After few steps (16) can be rewritten as

$$\boldsymbol{a}(\phi)\boldsymbol{\Lambda}\boldsymbol{a}^{\mathrm{H}}(\phi)\boldsymbol{s} = \boldsymbol{a}(\phi)\boldsymbol{\Lambda}f_d(\phi) \quad (17)$$

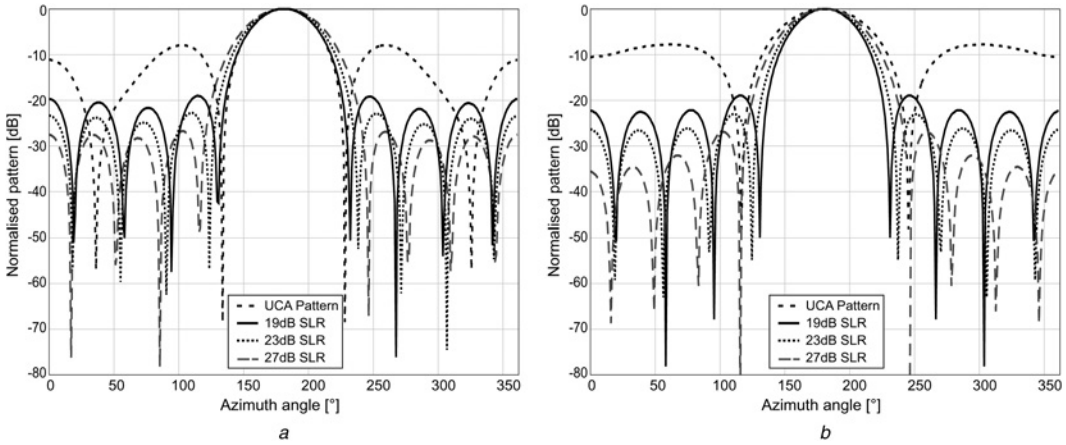

Fig. 6 *Results of the proposed SLR method*
a UCA with radius $r = 0.48\lambda$
b UCA with radius $r = 0.36\lambda$

which leads to the expression of the UCA steering vector

$$\boldsymbol{s} = \frac{\boldsymbol{a}(\phi)\boldsymbol{\Lambda} f_d(\phi)}{\boldsymbol{a}(\phi)\boldsymbol{\Lambda}\boldsymbol{a}^{\mathrm{H}}(\phi)} \tag{18}$$

Different $\boldsymbol{\Lambda}$ functions have been applied to (18), leading to different SLR levels. Results of the DBF algorithm, for two circular arrays with different radius lengths, are presented in Fig. 6, whereas the 3 dB beamwidth apertures of the synthesised patterns, with respect to the unweighted UCA excitations, are summarised in Table 2. The radius of $r = 0.36\lambda$ has been chosen as a comparison term as it shows, among the analysed cases, the best angular resolution of the array pattern. It is interesting to observe that for $r = 0.36\lambda$ the implemented DBF algorithm produces a slightly better angular resolution than the uniformly weighted case. On the other hand, an array radius of 0.48λ is still preferable with respect to the MC.

Table 2 Azimuthal resolution performances

	Uniform tapering	Proposed tapering		
SLR, dB	−8	−19	−23	−27
$r = 0.36\lambda$, °	57.6	41.6	45	50.2
$r = 0.48\lambda$, °	43	43	46.7	51.2

4.2 Comparison with the phase modes technique

The formulation of the phase mode excitations, whose proof is omitted as already published in literature [20], is given by

$$a_n = \sum_{p=-P}^{P} \frac{\mathrm{e}^{\mathrm{j}p(\phi_n - \phi_0)}}{j^p J_p(kr)} \tag{19}$$

being $P = \lfloor (N-1)/2 \rfloor$ and $J_p(\cdot)$ the first kind Bessel function of order p.

The tapering introduced by (19) produces a virtual transformation of the circularly shaped array into a linear array structure, resulting in a SLL of −13 dB. A secondary effect resides in the possibility of over-imposing a conventional tapering window in order to further reduce the SLL.

The phase mode weights with additive tapering windows have been applied to the circular arrays with different radius presented in the previous section. In Fig. 7 the obtained array patterns are shown whereas a comparison between the angular resolutions realised with the phase-mode excitations and the tapering of the proposed DBF algorithm is listed in Table 3.

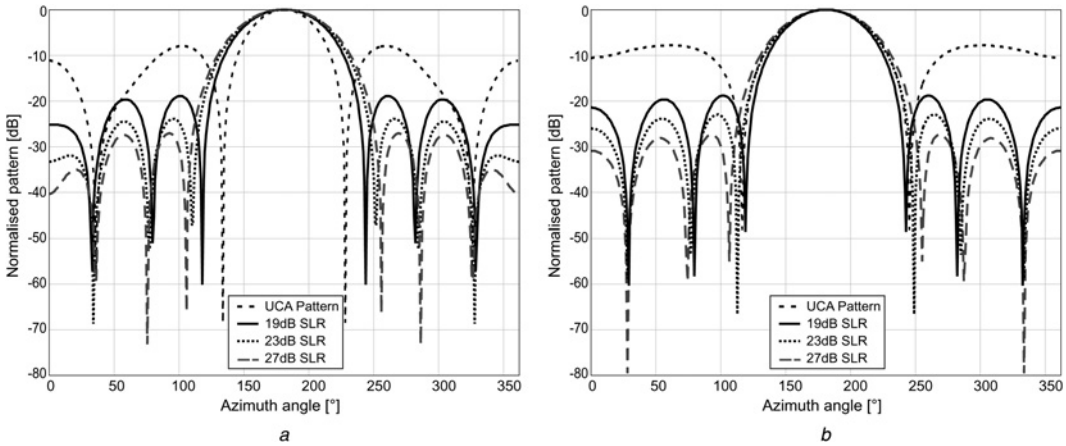

Fig. 7 *Results of the phase modes SLR method*
a UCA with radius $r = 0.48\lambda$
b UCA with radius $r = 0.36\lambda$

doi: 10.1049/iet-rsn.2011.0401

Table 3 Angular resolution comparison for different SLL taperings

		SLL reduction		
		−19 dB	−23 dB	−27 dB
$r = 0.36\lambda$	phase modes	53.2°	56.2°	59°
	proposed DBF	41.6°	45°	50.2°
$r = 0.48\lambda$	phase modes	55.7°	58.4°	60.9°
	proposed DBF	43°	46.7°	51.2°

Table 4 Illumination efficiency comparison for different SLL taperings

		SLL reduction		
		−19 dB	−23 dB	−27 dB
$r = 0.36\lambda$	phase modes	0.97	0.97	0.98
	proposed DBF	0.82	0.89	0.93
$r = 0.48\lambda$	phase modes	0.81	0.83	0.84
	proposed DBF	0.82	0.81	0.76

In both cases, for the different values of the radius length, and for all the obtained SLL reductions the proposed DBF method provides better angular resolutions than the phase modes technique. In order to better asses the validity of the proposed pattern synthesis method, the illumination efficiency of the array weights is also evaluated in the two cases. Being the efficiency η defined as

$$\eta = \frac{(\sum_{n=1}^{N} |a_n|)^2}{N \sum_{n=1}^{N} |a_n|^2} \tag{20}$$

the results for all the considered configurations are shown in Table 4.

With reference to the depicted values, on the one hand the proposed algorithm shows an improvement in terms of angular resolution 'gain' which is, on average, equal to 14.4%; on the other hand, the illumination efficiency is, also on average, 5.3% lower than the phase modes one. For the application purpose, because of the poor directivity of the circular array pattern, an improvement of the angular resolution is preferable. The quality of the proposed method is then confirmed. For the following processing steps, the tapering mask that ensures an SLL reduction of −19 dB has been used.

5 Digital signal and data processing

In this section we describe the main steps that are involved in the PCL processing. With reference to Fig. 8 after the signal digital conversion, the reference and the surveillance channel are synthesised via DBF. The surveillance channel acquisition is also characterised by the pattern nulling towards the reference direction; the DPI suppression is then completed by applying the gradient least mean squared (G-LMS) filter. Matched filtering (MF), constant false alarm rate (CFAR) thresholding and plot/data extraction complete the processing chain.

An integration time of 1 s and an equivalent pulse repetition frequency (PRF) of 244 Hz have been used for the signal processing.

5.1 Interference suppression

The DPI reduction is based on two different steps: the synthesis of an adapted pattern with a null in the direction of the reference illuminator and a digital filter which provides the further reduction of the DPI signal.

For a known direction of arrival of the direct signal, represented by the steering vector $\boldsymbol{v}$, the expression of the nulling matrix is given by

$$\boldsymbol{M}^{-1} = \frac{1}{\sigma_n^2}\left[\boldsymbol{I} - \frac{\boldsymbol{v}\boldsymbol{v}^{\mathrm{H}}}{1 + \boldsymbol{v}\boldsymbol{v}^{\mathrm{H}}}\right] \tag{21}$$

being σ_n^2 the noise variance. The surveillance channel $x_s(t)$, towards the direction described by the steering vector $\boldsymbol{s}$, is then defined by

$$x_s(t) = \boldsymbol{s}^{\mathrm{H}}\boldsymbol{M}^{-1}\boldsymbol{x} \tag{22}$$

where $\boldsymbol{x} = [x_1(t)\ x_2(t)\ \ldots\ x_8(t)]$ is the eight-channel output vector of digitalised data. According to the used notation, the reference signal is given by

$$x_r(t) = \boldsymbol{v}^{\mathrm{H}}\boldsymbol{x} \tag{23}$$

Experimental results have shown an effective suppression provided by the DBF nulling, because of the width of the array pattern, in the order of 25 dB. Fig. 9 presents a real example of the achieved suppression level; the digitally rotated resulting patterns, after calibration, SLR implementation and nulling procedure are also shown.

For conventional processing scenarios, which at best allow using 1 s of integration time for an effective bandwidth of 50 kHz, the autocorrelation function of an FM signal is characterised by range/Doppler sidelobes at a level of 40–50 dB. Given that the direct signal itself can be 80–90 dB higher than the expected reflection from a real target, it is clear that a suppression of 25 dB is not enough for the PCL system.

The further suppression of the residual direct signal $x_r(t)$ in the surveillance channel $x_s(t)$ can be achieved by a digital filtering subtraction. The implemented filtering procedure is based on an adaptive G-LMS filter [21] and, since the interference is not constant, the filter has to continuously adapt its coefficients to the interference variation. In the

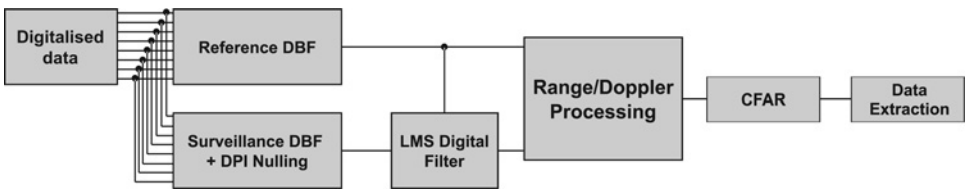

Fig. 8 *Signal and data processing scheme of the passive radar processing chain*

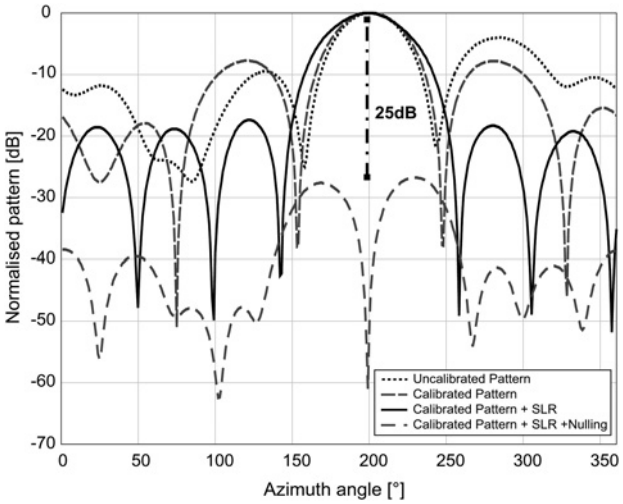

Fig. 9 *Effect of the DBF nulling procedure on the array pattern behaviour*

following description of the filter we use the discrete-time notation, with k as the time index.

At time instant k, the N tap-delayed inputs $\boldsymbol{x}_k = [x_k, \ldots, x_{k-N+1}]^{\mathrm{T}}$ of the reference signal are fed to the filter with weights $\boldsymbol{w}_k = [w_k(0), \ldots, w(N-1)]^{\mathrm{T}}$. The output signal at time k is then

$$y_k = \sum_{n=0}^{N-1} w_k^*(n) x_{k-n} = \boldsymbol{w}_k^{\mathrm{H}} \boldsymbol{x}_k \tag{24}$$

If we define the error signal e_k as the difference between the filtered signal y_k and the desired signal $d_k \equiv x_{\mathrm{s}}(t)$

$$e_k = d_k - \boldsymbol{w}_k^{\mathrm{H}} \boldsymbol{x}_x = d_k - y_k \tag{25}$$

the interference cancellation is realised when (25) is minimal. In order to minimise the error power, the weights vector $\boldsymbol{w}_k$ is adapted according to the LMS optimisation algorithm

$$\boldsymbol{w}_{k+1} = \boldsymbol{w}_k - \delta \frac{\partial e_k}{\partial \boldsymbol{w}_k} e_k = \boldsymbol{w}_k + \delta \boldsymbol{x}_k^{\mathrm{H}} e_k \tag{26}$$

Where the product $(\partial e_k / \partial \boldsymbol{w}_k) e_k$ represents the gradient of the function $(1/2)e_k^2$ and the scalar term δ is called the learning rate of the filter and it depends on the variability of the signal which must be removed. Experimental tests have shown that a learning rate $\delta = 0.005$ and a number of filter taps $N = 48$ are suitable values for this application. Typical additional suppression provided by the filter with the mentioned characteristics is in the order of 30–40 dB.

5.2 MF and greatest-of (GO)-CFAR detection

For both active and passive radar cases, the signal to be detected is a delayed and Doppler shifted copy of the transmitter/reference signal $x_{\mathrm{r}}(t)$. According to the theory, for a detailed derivation of which the reader is referred to the radar literature [22], the optimum detector output can be written as

$$Z(\tau, f_{\mathrm{D}}) = |z(\tau, f_{\mathrm{D}})|^2 = \left| \int_{-\infty}^{+\infty} x_s(t) x_{\mathrm{r}}^*(t-\tau) \mathrm{e}^{-\mathrm{j}2\pi f_D t} \, \mathrm{d}t \right|^2 \tag{27}$$

The formulation shows that the MF receiver is equivalent to the Fourier transform of the product between the surveillance channel signal and a delayed conjugate version of the reference signal. The software implementation makes use of this equivalence.

The amplitude values of (27) have been passed through a CFAR detector based on the GO principle [23]. The reference window size, in both range and Doppler dimensions, and the detection threshold were empirically estimated over different range/Doppler maps at the output of the MF. The estimation led to a (17×17) window, having therefore $M = 8$ cells on each side of the cell under test, with a threshold $\kappa_0 = 6$ dB. The threshold value has been chosen to increase the detection probability despite the reduced sensitivity of the system caused by the degraded noise figure. The higher false alarm rate was tolerated.

The outputs of the CFAR algorithm are shown in Figs. 10*a* and 11*a* for the range/time and range/Doppler cases, respectively.

The detection performances were compared with the track data provided by an ADS-B transponder and recorded at the same time of the experiment. By taking into account that this technology is not yet available on all the flights, only some of the detected tracks have a matching with the information included in the ADS-B files. The comparisons

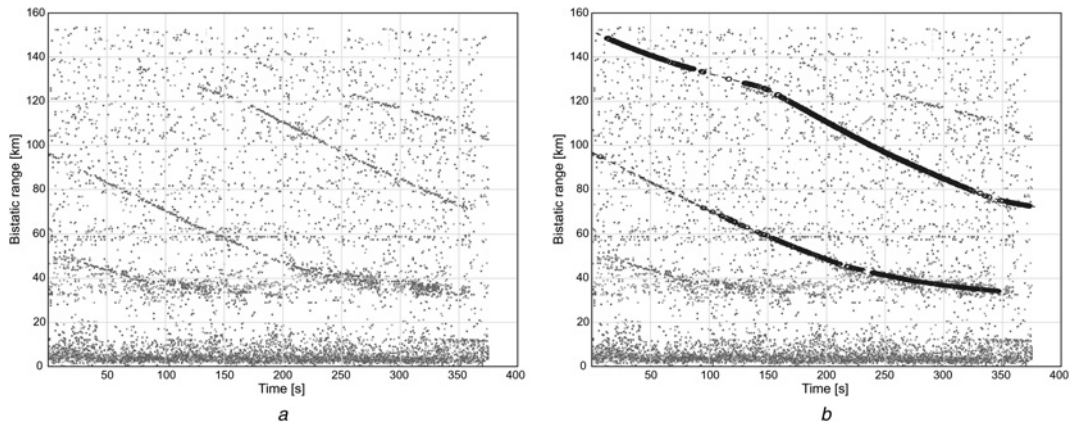

Fig. 10 *Comparison between the range/time radar output and the ground truth data*

a GO-CFAR detections

b Overlapping of the GO-CFAR detections with the ADS-B tracks

doi: 10.1049/iet-rsn.2011.0401

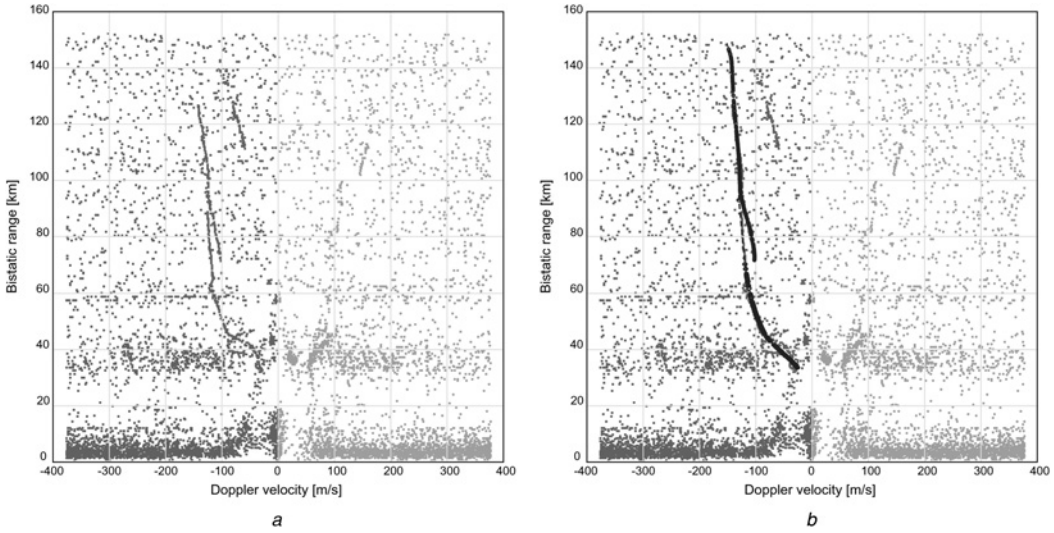

Fig. 11 *Comparison between the range/Doppler radar output and the ground truth data*

a GO-CFAR detections
b Overlapping of the GO-CFAR detections with the ADS-B tracks

between the detections and the ground truth data are illustrated in Figs. 10*b* and 11*b*. A good matching with the overall track evolution can be distinguished for the entire extension of the available data set.

6 Conclusions

In this paper the authors presented the set-up of a PCL radar system based on the exploitation of the FM broadcasters as transmitters of opportunity. The main aim of the research was to fully characterise the array section used for the passive radar system and to evaluate the benefits produced by *ad hoc* digital-processing techniques for the array calibration, the array pattern shaping and the DPI suppression.

Specifically: (i) the design of an agile analogue/digital receiver has been shown; (ii) the calibration steps followed to compensate for both system and MC errors have been outlined and experimental results have confirmed good performance in ideal pattern retrieval; (iii) a novel DBF method for the array pattern shaping was introduced and its results have been compared with the phase mode approach, an algorithm specifically tailored for circular arrays; the proposed shaping technique ensured better results in the angular resolution of the synthesised pattern, whereas a negligible reduction of illumination efficiency was calculated. Although the receiver is designed such to allow listening to multiple channels, in this paper the calibration and experimental validation for a single channel has been presented.

Finally, the acquisition of ADS-B data allowed assessing the detection capabilities of the PCL, therefore providing a performance verification of the proposed design. According to the overall analysis that has been presented, some future improvements have been identified for the system. The achieved angular resolution, when only electronic steering is performed, is obviously below the standard expected from a surveillance radar system. A clear improvement from this point of view can be obtained by exploiting high-resolution techniques based on either monopulse or spectral estimation approaches. The use of the available agile receiver will be realised by upgrading the data acquisition LAN; in this way an effective multilateral system can be obtained, with an expected gain in terms of radar coverage and resolution both in range and angle. A higher sensitivity can be achieved by reducing the actual noise figure of the receiver, which is currently degraded by the need of a double attenuation step in the RF section of the receiver in order to avoid the clipping during the digital conversion. State-of-the-art PC digitiser boards will be installed into the PCL working station to overcome this problem. Different digital processing algorithms will also be taken into account in order to mitigate the false alarms, which is an important issue for an improved performance of the tracker.

7 Acknowledgments

The authors thank Dr. Sjoerd J. Gelsema from the NATO Consultation, Command and Control Agency (NC3A) for the provision of the ADS-B data which were used in the trial. The experimental data collection has been performed at and with the support of the TNO, the Netherlands. The authors would like to thank Arne Theil, Duije Deurloo and Frans Nennie from TNO for their help in the data processing algorithms development, the radar receiver design and the circular array parameter measurements respectively.

8 References

1 Howland, P.E., Maksimiuk, D., Reitsma, G.: 'FM radio based bistatic radar', *IEE Proc. Radar Sonar Navig.*, 2005, **152**, (3), pp. 107–115
2 Fabrizio, G., Colone, F., Lombardo, P., Farina, A.: 'Adaptive beamforming for high-frequency over-the-horizon passive radar', *IET Radar Sonar Navig.*, 2009, **3**, (4), pp. 384–405
3 Griffiths, H.D., Long, N.R.W.: 'Television based bistatic radar', *IEE Proc. F, Commun. Radar Signal Proc.*, 1986, **133**, (7), pp. 649–657
4 Poullin, D.: 'Passive detection using digital broadcasters (DAB, DVB) with COFDM modulation', *IEE Proc. Radar Sonar Navig.*, 2005, **152**, (3), pp. 143–152
5 Willis, N.J.: 'Bistatic radar' (SciTech Publishing Inc., 2005)
6 Willis, N.J., Griffiths, H.D.: 'Advances in bistatic radar' (SciTech Publishing Inc., 2007)
7 Griffiths, H.D., Baker, C.J.: 'Passive coherent location radar systems. Part 1: performance prediction', *IEE Proc. Radar, Sonar Navig.*, 2005, **152**, (3), pp. 153–159
8 Baker, C.J., Griffiths, H.D., Papoutsis, I.: 'Passive coherent location radar systems. Part 2: waveform properties', *IEE Proc. Radar, Sonar Navig.*, 2005, **152**, (3), pp. 160–168

9 O'Hagan, D., Colone, F., Baker, C.J., Griffiths, H.D.: 'Passive bistatic radar (PBR) demonstrator'. IET Int. Conf. Radar Systems, Edinburgh, UK, October 2007, pp. 1–5
10 Howland, P.E.: 'Target tracking using television-based bistatic radar', *IEE Proc. Radar, Sonar Navig.*, 1999, **146**, (3), pp. 166–174
11 Malanowski, M., Kulpa, K.: 'Digital beamforming for passive coherent location radar'. IEEE Radar Conf., Rome, Italy, May 2008, pp. 1–6
12 Ecrin Systems, http://www.ecrin.com/datasheets/GEFIP/ics-554.pdf
13 CST–Computer Simulation Technology, http://www.cst.com
14 Steyskal, H., Herd, J.S.: 'Mutual coupling compensation in small array antennas', *IEEE Trans. Antennas Propag.*, 1990, **38**, (12), pp. 1971–1975
15 Balanis, C.A.: 'Antenna theory: analysis and design' (Wiley Interscience, 2005, 3rd edn.)
16 Shanno, D.F.: 'Conditioning of quasi-Newton methods for function minimization', *Math. Comput.*, 1970, **24**, (111), pp. 647–656
17 Broyden, C.G.: 'The convergence of a class of double-rank minimization algorithms', *IMA J. Instit. Math. Appl.*, 1970, **6**, pp. 222–231
18 Mailloux, R.J.: 'Phased array antenna handbook' (Artech House, 2005, 2nd edn.)
19 Thadeu Freitas de Abreu, G., Kohno, R.: 'A modified Dolph-Chebyshev approach for the synthesis of low sidelobe beampatterns with adjustable beamwidth', *IEEE Trans. Antennas Propag.*, 2003, **51**, (10), pp. 3014–3017
20 Rahim, T., Davies, D.E.N.: 'Effect of directional elements on the directional response of circular antenna arrays', *IEE Proc. H, Microw. Opt. Antennas*, 1982, **129**, (1), pp. 18–22
21 Haykin, S.: 'Adaptive filter theory' (Prentice Hall Information and Systems Sciences Series, Prentice Hall, 2002, 4th edn.)
22 Skolnik, M.I.: 'Radar handbook – 2nd edn' (McGraw-Hill, 1990)
23 Rohling, H.: 'Radar CFAR thresholding in clutter and multiple target situations', *IEEE Trans. Aerosp. Electron. Syst.*, 1983, **AES-19**, (4), pp. 608–621

doi: 10.1049/iet-rsn.2011.0401